

# RSC Advances



This is an *Accepted Manuscript*, which has been through the Royal Society of Chemistry peer review process and has been accepted for publication.

*Accepted Manuscripts* are published online shortly after acceptance, before technical editing, formatting and proof reading. Using this free service, authors can make their results available to the community, in citable form, before we publish the edited article. This *Accepted Manuscript* will be replaced by the edited, formatted and paginated article as soon as this is available.

You can find more information about *Accepted Manuscripts* in the [Information for Authors](#).

Please note that technical editing may introduce minor changes to the text and/or graphics, which may alter content. The journal's standard [Terms & Conditions](#) and the [Ethical guidelines](#) still apply. In no event shall the Royal Society of Chemistry be held responsible for any errors or omissions in this *Accepted Manuscript* or any consequences arising from the use of any information it contains.

Graphene layers on bimetallic Ni/Cu(111) surface and near  
surface alloys in controlled growth of graphene

Xin Bian <sup>a</sup>, Qiang Wang <sup>a,\*</sup>, Xinyan Wang <sup>a,d</sup>, Lu Wang <sup>a</sup>, Wei-qi Li <sup>b</sup>, Guang-hui  
Chen <sup>c</sup>, and Hongjun Zhu <sup>a,\*</sup>

<sup>a</sup>Department of Applied Chemistry, College of Chemistry and Molecular  
Engineering, Nanjing Tech University, Nanjing 211816, P. R. China

<sup>b</sup>Department of Physics, Harbin Institute of Technology, Harbin 150001, P. R. China

<sup>c</sup>Department of Chemistry, Shantou University, Shantou, Guangdong, 515063, P. R.  
China

<sup>d</sup>Technology Center, Shanghai Meishan Iron & steel CO. Ltd., Nanjing, Jiangsu  
210039, P. R. China

\*Corresponding author.

E-mail address: [wangqiang@njtech.edu.cn](mailto:wangqiang@njtech.edu.cn) (Qiang Wang)

[zhuhj@njtech.edu.cn](mailto:zhuhj@njtech.edu.cn) (Hongjun Zhu)

Tel. / Fax: + 86-25-83172358

**Abstract**

Bimetallic alloy is more effective than pure metal for controlled growth of high-quality graphene. In this work, we used the DFT-D2 method to study interfacial structure, interaction between graphene layers and bimetallic Ni/Cu(111) surface and near-surface alloys (SAs, NSAs). The results show that the bimetallic Ni/Cu(111) SAs and NSAs have a larger surface relaxation and charge transfer at interface. The Ni/Cu(111) SAs/NSAs with Cu-surface layer are energetically more favorable than that with Ni-surface layer. However, the Ni-surface layer of the Ni/Cu(111) SAs/NSAs has more charge accumulation and higher chemical activity than the Cu-surface layer of the Ni/Cu(111) SAs/NSAs. More importantly, the interaction strength of graphene-metal can be distinctly tuned by surface alloying, while it has only minor change by subsurface alloying. The initially weak interfacial interaction of graphene/Cu(111) could be enhanced substantially by Ni surface introducing. Accordingly, the interface distance was decreased from  $\sim 3.0$  Å to  $\sim 2.1$  Å, and there is a strong charge transfer from the Ni-surface layer to graphene bottom layer. In contrast, the initially strong interfacial interaction of graphene/Ni(111) could be reduced successfully by Cu surface introducing. The interface distance was increased from  $\sim 2.1$  Å to  $\sim 3.0$  Å, and there is only a minor electronic polarization at interface between graphene and Ni(111)-Ni-Cu SA. Furthermore, the graphene bottom layer on the Ni-surface layer of the Ni/Cu(111) SA/NSAs has higher chemical activity than that on Cu-surface layer of the Ni/Cu(111) SA/NSAs. These findings provide a useful guide for designing alloy catalyst and achieving controlled growth of graphene.

**KEYWORDS:** Ni/Cu(111) bimetallic alloys, graphene layer, interaction strength, charge transfer, DFT-D2 calculation

## Introduction

Epitaxial growth of graphene on transition metal surfaces has been one of the most commonly used methods for producing large-area graphene with high-quality.<sup>1-4</sup> Many efforts have been devoted to growing monolayer, bilayer or few-layer graphene by chemical vapor deposition method on various metal substrates, such as Ni,<sup>5-7</sup> Cu,<sup>8-10</sup> Ru,<sup>11, 12</sup> and Ir.<sup>13, 14</sup> Among them, Ni and Cu have been widely used to grow the large-area and high-quality graphene films.<sup>5-10</sup> Experiment studies have reported that graphene of different layers has been grown on Ni, Cu, and Ni/Cu alloy.<sup>10, 15-17</sup> It is proposed that graphene growth on Ni surfaces is a C segregation or precipitation process,<sup>5</sup> while graphene growth on Cu surfaces is a catalytic, self-limiting process because of the low solubility of carbon in copper.<sup>8-10, 18, 19</sup> Growth on Ni surface usually leads to a mixture of various layers graphene, whereas Cu surface is suitable for growing mono- or bilayer graphene.<sup>17, 20-22</sup> Cu/Ni alloys, a combination of the well-behaved Ni and Cu, was used to achieve layer controlled growth of graphene by fine tuning the atomic percentage of Ni in Cu/Ni alloy.<sup>23, 24</sup>

Recently, several studies have reported the properties and Morphologies of the graphene grown on metal surfaces strongly depend on the interfacial interaction between graphene layers and metal surfaces.<sup>15, 23, 25, 26</sup> Generally, a strong interaction between the graphene and metal surface would easily grow multilayer graphene with various defects, and difficultly transfer in the post processing, such as chemisorbed Ni<sup>5, 25</sup> and Co<sup>27, 28</sup>. A weak interaction between the graphene and metal surface is favorable to grow the uniform monolayer graphene, such as physisorbed Cu.<sup>25</sup> However, it easily results in stopping growth of the second layer once the catalytic surface is fully covered with one layer graphene.<sup>25</sup> Thereby, it is highly desirable to tune graphene-metal interaction by bimetallic SA/NSAs, which are synthesized

experimentally by depositing one of the two metals on the surface of the other metal.<sup>23, 29-31</sup> Experimental studies have demonstrated that the metal alloys are more effective than pure metals for controlled growth of high-quality graphene.<sup>24</sup> Several groups revealed the interaction strength of graphene-Ni substrate could be weakened by intercalating Cu,<sup>32</sup> Au,<sup>33</sup> and Sn.<sup>30</sup> Meanwhile, Liu *et al.* reported that monolayer and bilayer graphene could be controlled growth on the Ni/Cu alloys by deposition of Ni atoms onto Cu surface.<sup>23</sup> The interactions of heteronuclear metal-metal and graphene-metal are important during the process of graphene growth, and their understanding is the basis for controlled growth of high-quality graphene. Besides, it is also useful to study the graphene-metal interface for designing high performance graphene based electronic and optoelectronic devices.<sup>34</sup>

In this study, we choose the semi-empirical DFT-D2 Grimme's method,<sup>35, 36</sup> which includes long-range van der Waals (vdW) forces, to study the properties of the Ni/Cu(111) SAs and NSAs and their interaction with various graphene layers. Points of fundamental interest are to elucidate the nature of the surface geometry, electronic structure, chemical reactivity, and interaction behavior of these bimetallic Ni/Cu(111) SAs and NSAs with various graphene layers, and further compare the differences of graphene layers on the mono- and bi-metallic surfaces.

### Computational methods

Spin-polarized computations were performed with the projector augmented wave (PAW) method<sup>37, 38</sup> for electron-ion interactions using the VASP code.<sup>39</sup> The exchange-correlation interaction was treated in the general gradient approximation (GGA)<sup>40, 41</sup> in the parameterization of Perdew-Burke-Ernzerhof (PBE).<sup>42</sup> Long-range dispersion corrections have been considered within the DFT-D2 method. The dispersion coefficient  $C_6$  and vdW radius  $R_0$  for C, Ni, and Cu used in our DFT-D2

method were taken from previous work.<sup>35, 36</sup> The scale factor  $S_6$  was 0.75.<sup>43, 44</sup> The cutoff energy for the plane-wave basis set was set to 400 eV. The electronic self-consistency criterion has been set to  $10^{-6}$  eV.

To simulate the Ni/Cu(111) SAs and NSAs, the Ni(111)-Ni-Cu, Ni(111)-Cu-Ni, Cu(111)-Cu-Ni and Cu(111)-Ni-Cu were modeled as the periodic slab geometry, which were built by substituting the surface or subsurface layer of the Ni(111) or Cu(111) with single Cu or Ni layer. Each 1 x 1 super cell contains six atomic layers of metal atoms and a vacuum region. These Ni/Cu(111) SA/NSAs were firstly relaxed, and then various graphene structures were placed in the vacuum region on top of the Ni/Cu(111) SAs/NSAs as shown in Fig. 1, Each vacuum region was at least 15 Å in the direction perpendicular to the interface to avoid interaction with their own images. The Brillouin-zone integrations were done with a  $21 \times 21 \times 1$  k-point mesh for geometry optimizations and a  $36 \times 36 \times 1$  k-point mesh for electronic properties, respectively.<sup>45</sup> The bottom two layers of the Ni/Cu(111) SA/NSAs were fixed, while other four metal layers and graphene layers were allowed to relax during geometry optimization. Lattice mismatches between graphene and bimetallic surfaces were 0.8% for Ni-based substrates and 2.0% for Cu-based substrates, respectively. Since the lattice mismatches of graphene and bimetallic surfaces are relatively small, there is only a small influence on the adsorption strength and charge transfer. The global transferred charges were calculated by the atomic Bader charge analysis.<sup>35, 46, 47</sup>

The adsorption energy per carbon atom of graphene structures on Ni/Cu(111) SA/NSAs surfaces is calculated by  $\Delta E_{gM} = (E_{gM} - (E_g + E_M)) / 2$ , where 2 is the number of carbon atoms in each graphene layer per super cell.  $E_{gM}$ ,  $E_g$ , and  $E_M$  are the total energies of the graphene-Ni/Cu(111) systems, freestanding mono-, bi- and tri-layer graphene and bimetallic SA/NSA systems per super cell, respectively.

## Results

### Geometric structure

Fig. 1a shows optimized geometric structures of free mono-, bi-(AA and AB), trilayer (ABA and ABC) graphene with different stacking sequences. Each super cell includes two C atoms in each graphene layer (as the blue dashed line in Fig. 1a). The C-C bond length in freestanding graphene layer is 1.42 Å, while the C-C bond length is compressed to 1.41 Å on Ni-surface layer and stretched to 1.46 Å on Cu-surface layer of graphene-Ni/Cu(111) SA/NSA systems (as listed in Table 2), respectively.

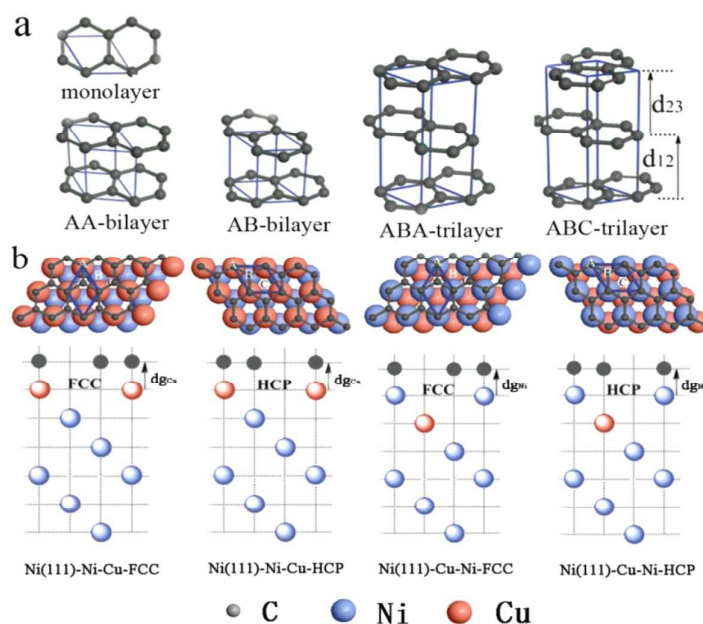


**Fig. 1** Optimized geometric structures of (a) freestanding mono-, bi- (AA and AB stacking) and trilayer (ABA and ABC stacking) graphene, (b) the side and top views of monolayer graphene absorbed on Ni/Cu(111) SAs and NSAs. The blue lines mark super cell.  $d_{12}$  and  $d_{23}$  are the interlayer distances between two graphene layers, and  $d_{g^{Cu/Ni}}$  is the distance between the graphene bottom layer and alloy surface.

**Table 1** Interlayer vertical distance ( $d_{nm}$ , Å) at z direction between two metal layers for pure Ni(111), Cu(111), and Ni/Cu(111) SAs/NSAs.

	$d_{12}$	$d_{23}$	$d_{34}$	$d_{45}$	$d_{56}$
Ni(111)	1.99	1.99	2.00	2.00	1.99
Ni(111)-Ni-Cu	2.06	2.00	1.99	1.99	1.99
Ni(111)-Cu-Ni	2.05	2.06	1.99	1.99	1.99

Cu(111)-Ni-Cu	2.01	2.01	2.06	2.07	2.08
Cu(111)-Cu-Ni	2.00	2.06	2.07	2.07	2.08
Cu(111)	2.08	2.06	2.07	2.06	2.08

Table 1 shows the interface vertical distance between two metal layers of these bimetallic Ni/Cu(111) SAs and NSAs. There is a distinct surface relaxation for these Ni/Cu(111) SAs and NSAs. The interlayer distance increases when a Ni layer of the Ni(111) is substituted with a Cu layer. The interlayer distance of the Ni(111)-Ni-Cu SA,  $d_{12}$ , is 2.06 Å, longer than that of the Ni(111) by 0.07 Å as listed in Table 1. Similarly, the interlayer distances of the Ni(111)-Cu-Ni NSA,  $d_{12}$  and  $d_{23}$ , are also longer than that of the Ni(111) by ~0.06 Å, respectively. In contrast, it decreases when a Cu layer of the Cu(111) is substituted with a Ni layer. The interlayer distance of the Cu(111)-Cu-Ni SA,  $d_{12}$ , is shorter than that of the Cu(111) by 0.08 Å. For the Cu(111)-Ni-Cu NSA, the interlayer distances,  $d_{12}$  and  $d_{23}$ , are also shorter than that of the Cu(111) by 0.07 and 0.05 Å, respectively. However, the interlayer distances among underlying metal layers has no significant changes in these Ni/Cu(111) SAs and NSAs.

#### Stability of bimetallic Ni/Cu(111) SAs and NSAs

Next, the relatively thermodynamic stability of these bimetallic Ni/Cu(111) SAs and NSAs were compared. The results show that the Ni(111)-Ni-Cu SA is energetically more favorable than the Ni(111)-Cu-Ni NSA by 0.04 eV/atom. In contrast, the Cu(111)-Cu-Ni SA is energetically unfavorable than the Cu(111)-Ni-Cu NSA by 0.03 eV/atom. The results indicate that the Cu tends to segregate to the surface, while Ni prefers to enrich in the subsurface layers for the Ni/Cu alloys. Recently, The bimetallic Ni/Cu(111) SAs and NSAs have been produced by deposition one of two metals on the (111) surface of the other metal.<sup>48</sup> The results show that the bimetallic Ni/Cu(111) SA/NSAs with Cu-surface layers are

thermodynamically more favorable than that with the Ni-surface layers due to the higher surface free energy of nickel. The Cu(111)-Cu-Ni SA is thermodynamically stable until 450 K. Subsequently, the Cu component of the Cu(111)-Cu-Ni would segregate to surface, and further form a Cu(111)-Ni-Cu NAS at higher temperature. However, the Ni(111)-Ni-Cu SA starts segregating until 800K, and forms a Ni(111)-Cu-Ni mixed SA finally.<sup>48</sup> Furthermore, the bimetallic Ni@Cu and Cu@Ni core-shell particles have been also synthesized successfully. The Ni@Cu particles with Cu-shell structure have been substantiated thermodynamically more favorable than the Cu@Ni particles with Ni-shell structure. The Cu component of the Cu@Ni core-shell particles tends to segregate to the surface during elevated temperature.<sup>49</sup>

Theoretically, a recent study also showed that the Ni(111)-Cu-Ni NSA was energetically less stable than the Ni(111)-Ni-Cu SA by 0.05 eV/atom.<sup>24</sup> However, the relative thermodynamic stability of the Ni(111)-Cu-Ni and Ni(111)-Ni-Cu could be reversed upon carbon atoms adsorption during initial stage of graphene nucleation. They found that the Ni(111)-Cu-Ni NSA was energetically more stable than the Ni(111)-Ni-Cu SA by 0.01 eV/atom once the single carbon adsorbed on their surfaces.<sup>24</sup> Thereby, in this work, the four bimetallic Ni/Cu(111) SAs and NSAs were all used.

### **Charge transfer and chemical activity of bimetallic Ni/Cu(111) SAs and NSAs**

It is well known that copper has a completely filled 3d-band and a partially filled 4s-band (Cu,  $3d^{10}4s^1$ ), while nickel has a partially filled 3d-band and a completely filled 4s-band (Ni,  $3d^84s^2$ ). Thus, electron tends to transfer from the 4s-band of copper to the 3d-band of nickel in the Ni/Cu alloys. Inspecting the interfaces of these bimetallic Ni/Cu(111) SAs and NSAs, we find that charge always transfers from Cu layer to Ni layer (see Fig. 2a, b, c, d and Table S1, SI). Furthermore, when Ni locates

at surface and Cu locates at subsurface, charge transfer would enhance from Cu to Ni because of synergistic combination of the surface effect and the electronic structure effect. For the Cu(111)-Cu-Ni SA, charge transfers from subsurface Cu (+0.06 e/atom) to surface Ni (-0.06 e/atom) as rendered in Fig. 2a. Interestingly, for the Ni(111)-Cu-Ni NSA as shown in Fig. 2b, when Cu locates at subsurface, charge evidently transfers from subsurface Cu (+0.06 e/atom) to surface Ni (-0.04 e/atom) and third Ni (-0.02 e/atom) layers, respectively. The Bader charge analysis further confirms that charge accumulation at surface layer follows the order Ni(111) (-0.03 e/atom) < Ni(111)-Cu-Ni (-0.04 e/atom) < Cu(111)-Cu-Ni (-0.06 e/atom).

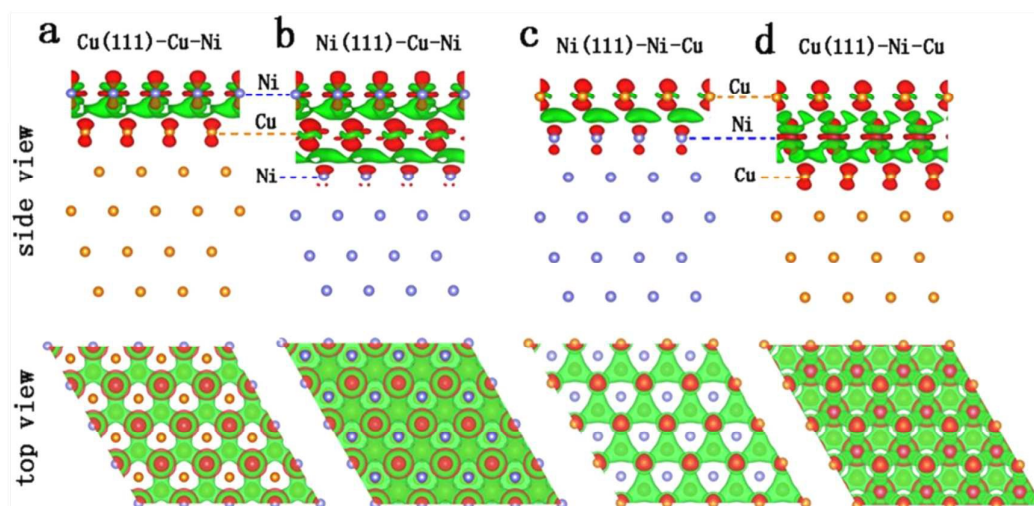


**Fig. 2** Charge density difference plots of the Ni/Cu(111) SAs and NSAs. The charge density difference refers to the variance between the total charge density of the Ni/Cu(111) and the sum of the charge density of the separated Cu (or Ni) single layer and other five Ni (or Cu) layers, which are kept the same geometric structures as those in the Ni/Cu(111) SAs and NSAs. The red and green color regions mark the depletion and accumulation of electronic charges, respectively. The top view shows the charge density difference at interface of the Ni/Cu(111) SAs and NSAs.

In contrast, when Cu locates at the surface, the charge transfer would decrease due to mutually offset of the surface effect and electronic structure effect. As shown in Fig. 2c, for the Ni(111)-Ni-Cu SA, charge accumulation at surface Cu layer is almost

0.00 e/atom, and -0.01 and +0.01 e/atom for the second and third Ni layers, respectively. While, for the Cu(111)-Ni-Cu NSA, charge distinctly accumulates at subsurface Ni layer (-0.04 e/atom), which transfers from the surface (+0.01 e/atom), third (+0.02 e/atom) and fourth (+0.01 e/atom) Cu layers, respectively. Charge accumulation at surface layer follows the order Cu(111)-Ni-Cu (+0.01 00e/atom) < Ni (111)-Ni-Cu (0.00 e/atom) < Cu (111) (-0.02 e/atom).

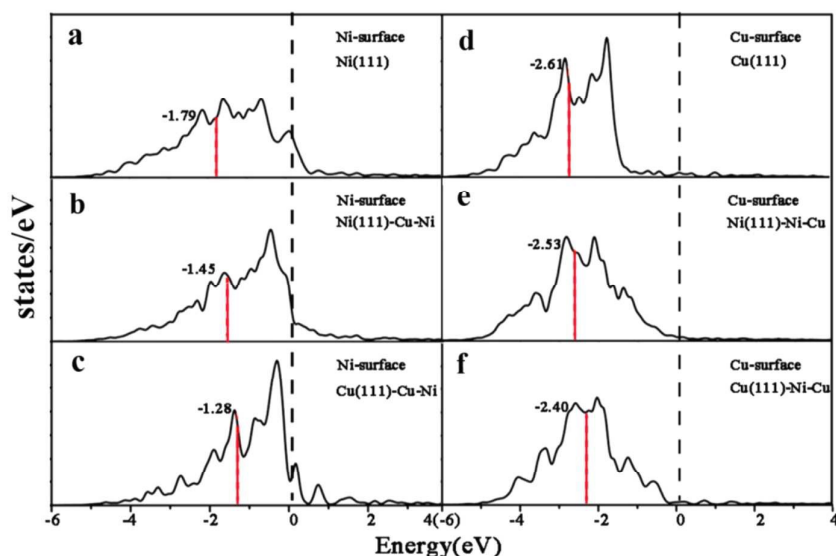


**Fig. 3** The density of states onto the d-band of the surface layer for the Ni(111), Cu(111) and Ni/Cu(111) SAs and NSAs. The red lines indicate the corresponding d-band center (eV). The dash lines represent the Fermi level, which is taken as zero.

In order to further understand charge-transfer-induced surface reactivity, the electron density analysis was performed to determine the density of states (DOS) onto the d-band of the surface layer for these Ni/Cu(111) SAs and NSAs. As shown in Fig. 3, the d-state curves of the surface layer show that Cu-surface layers have hardly any electron density near the Fermi level, whereas Ni-surface layers have stronger charge density near the Fermi level, which indicates the Ni/Cu(111) SA/NSAs with Ni-surface layer have the higher chemical activity than that with Cu-surface layer. Furthermore, it can be seen that the d-band states of the Ni-surface layer have larger

shift toward the Fermi level, which from -1.79 (Ni(111)) to -1.45 (Ni(111)-Cu-Ni), and to -1.28 eV (Cu(111)-Cu-Ni), as shown in Fig. 3a, b, and c. While the d-states of the Cu-surface layer have only slightly shift toward the Fermi level, which from -2.61 (Cu(111)) to -2.53 (Ni(111)-Ni-Cu), and to -2.40 eV (Cu(111)-Ni-Cu), as shown in Fig. 3d, e, and f. The results indicate the surfaces of these Ni/Cu(111) SAs and NSAs all have the higher chemical activity than their corresponding the Ni(111) and Cu(111) surfaces.

### **Graphene layers on Ni/Cu (111) SAs and NSAs**

#### **Adsorption energy**

In this section, we focus on the interaction behavior of these Ni/Cu(111) SAs and NSAs with various graphene layers, and then compared to the Ni(111) and Cu(111). As shown in Fig. 1b, two stable symmetrical configurations, FCC and HCP, were studied in this work. The detailed optimized structure parameters and corresponding adsorption energies are given in Table 2 and 3, respectively.

The results in Table 2 and 3 show that the interaction behavior of various graphene layers with different stacking sequence on the Ni/Cu(111) SAs and NSAs directly depend on the adjoining surface-metal layer. As illustrated in Table 2, the interlayer distances from the graphene bottom layer to the Cu-surface layer of the Ni(111)-Ni-Cu and Cu(111)-Ni-Cu are similar ( $d_{\text{gCu}}$ ,  $3.00 \pm 0.05 \text{ \AA}$ ), which are comparable to that in graphene/Cu(111) systems. The interlayer distances from the graphene bottom layer to the Ni-surface layer of the Cu(111)-Cu-Ni and Ni(111)-Cu-Ni are  $2.10 \pm 0.05 \text{ \AA}$ , which are comparable to that in graphene/Ni(111) systems. The interlayer distances from the bottom layer to the second layer ( $d_{12}$ ) and the second layer to the third layer of graphene ( $d_{23}$ ) are comparable to those of freestanding graphene layers.

**Table 2** Optimized structure parameters of freestanding mono-, bi-, and trilayer graphene, as well as these graphene layers adsorbed on N/Cu(111) SAs and NSAs.  $b$  is the C-C bond length in graphene.  $d_{12}$  and  $d_{23}$  are the interlayer distances from the bottom to second, and second to third layer.  $d_{gm}$  is the distance from the graphene bottom layer to surface layer of the Ni/Cu (111) SAs and NSAs. All values are given in Å.

Stacking	Monolayer		Bilayer				Trilayer				
			AB	AA	ABA	ABC					
Free	$d_{23}$	-	-	-	3.28	3.24					
	$d_{12}$	-	3.24	3.49	3.28	3.23					
	$b$	1.42	1.42	1.42	1.42	1.42					
Location		FCC	HCP	FCC	HCP	FCC	HCP	FCC	HCP	FCC	HCP
Ni(111)-Ni-Cu	$b$	1.46	1.46	1.46	1.46	1.46	1.46	1.46	1.46	1.46	1.46
	$d_{23}$	-	-	-	-	-	-	3.20	3.25	3.23	3.22
	$d_{12}$	-	-	3.20	3.19	3.45	3.47	3.21	3.25	3.23	3.20
	$d_{gCu}$	3.02	3.05	2.99	3.00	3.01	3.01	2.95	2.97	2.94	2.98
Ni(111)-Cu-Ni	$b$	1.41	1.41	1.41	1.41	1.41	1.41	1.41	1.41	1.41	1.41
	$d_{23}$	-	-	-	-	-	-	3.21	3.22	3.22	3.24
	$d_{12}$	-	-	3.15	3.14	3.26	3.28	3.15	3.17	3.16	3.17
	$d_{gNi}$	2.16	2.16	2.13	2.14	2.12	2.14	2.11	2.12	2.11	2.11
Cu(111)-Ni-Cu	$b$	1.46	1.46	1.46	1.46	1.46	1.46	1.46	1.46	1.46	1.46
	$d_{23}$	-	-	-	-	-	-	3.26	4.12	3.25	3.29
	$d_{12}$	-	-	3.26	3.30	3.50	3.52	3.25	3.25	3.24	3.24
	$d_{gCu}$	2.97	2.97	2.92	2.99	2.89	2.91	3.01	3.02	3.01	3.05
Cu(111)-Cu-Ni	$b$	1.41	1.41	1.41	1.41	1.41	1.41	1.41	1.41	1.41	1.41
	$d_{23}$	-	-	-	-	-	-	3.22	3.23	3.23	3.25
	$d_{12}$	-	-	3.17	3.20	3.30	3.34	3.15	3.16	3.15	3.17
	$d_{gNi}$	2.06	2.07	2.06	2.06	2.05	2.06	2.08	2.09	2.08	2.09

**Table 3** The adsorption energy (eV/C) of graphene layers on Ni(111), Cu(111) and Ni/Cu(111) SAs and NSAs. Adsorption locations correspond to the illustration in Fig. 1

Stacking	Monolayer		Bilayer				Trilayer			
			AB		AA		ABA		ABC	
Location	FCC	HCP	FCC	HCP	FCC	HCP	FCC	HCP	FCC	HCP
$\Delta E_{gNi(111)}$	-0.31	-0.30	-0.36	-0.35	-0.37	-0.35	-0.38	-0.36	-0.37	-0.35
$\Delta E_{gNi(111)-Cu-Ni}$	-0.29	-0.30	-0.35	-0.35	-0.36	-0.35	-0.37	-0.37	-0.37	-0.36
$\Delta E_{gCu(111)-Cu-Ni}$	-0.34	-0.34	-0.35	-0.34	-0.36	-0.35	-0.31	-0.29	-0.30	-0.29
$\Delta E_{gNi(111)-Ni-Cu}$	-0.22	-0.22	-0.25	-0.25	-0.24	-0.24	-0.27	-0.26	-0.26	-0.26
$\Delta E_{gCu(111)-Ni-Cu}$	-0.19	-0.19	-0.17	-0.16	-0.18	-0.17	-0.13	-0.13	-0.12	-0.11
$\Delta E_{gCu(111)}$	-0.19	-0.19	-0.17	-0.17	-0.16	-0.16	-0.14	-0.13	-0.13	-0.12

Importantly, the interaction strength between graphene bottom layer and surface-metal layer can be tuned by the Ni/Cu(111) SAs distinctly, while it has only a minor change when these graphene layers adsorb on the Ni/Cu(111) NSAs. As shown in Table 3, the adsorption energies of the graphene layers with different stacking sequence on the Ni(111)-Ni-Cu SA are significantly lower than that on the Ni(111) about 0.08~0.13 eV/C, but higher than that on the Cu(111) about 0.03~0.14 eV/C, respectively. In addition, the adsorption energies of these graphene layers adsorb on the Ni(111)-Ni-Cu have a similar change trend with that on the Ni(111), which increase with the increase of graphene layers: monolayer (~0.22 eV/C) < bilayer (~0.24 eV/C) < trilayer (~0.26 eV/C). However, no significant differences are found in the adsorption energies of these graphene layers on the Ni(111)-Cu-Ni NAS by comparing with that on the Ni(111). The adsorption energies have the same change trend with that on the Ni(111), which increase with the increase of graphene layers: monolayer (~0.30 eV/C) < bilayer (~0.35 eV/C) < trilayer (~0.37 eV/C).

When monolayer graphene adsorbs on the Cu(111)-Cu-Ni SA, the adsorption energies are 0.34 eV/C, which are even higher than that on the Ni(111) by 0.03 eV/C. The adsorption energies of bilayer graphene on Cu(111)-Cu-Ni are 0.35 eV/C, almost equal to that on the Ni(111). The adsorption energies of trilayer graphene on Cu(111)-Cu-Ni are 0.30 eV/C which lower than that on the Ni(111) surface by 0.07 eV. However, the adsorption energies of these graphene layers on the Cu(111)-Ni-Cu NSA are nearly equal to that on the Cu(111), and their change trend are also similar to that on the Cu(111), which decrease with the increase of graphene layers: monolayer (~0.19 eV/C) < bilayer (~0.17 eV/C) < trilayer (~0.12 eV/C). The adsorption energies difference between the FCC and HCP configurations of these graphene layers on these bimetallic SAs and NASs are insignificant.

### Charge transfer in the graphene-Ni/Cu(111) SA and NSA systems

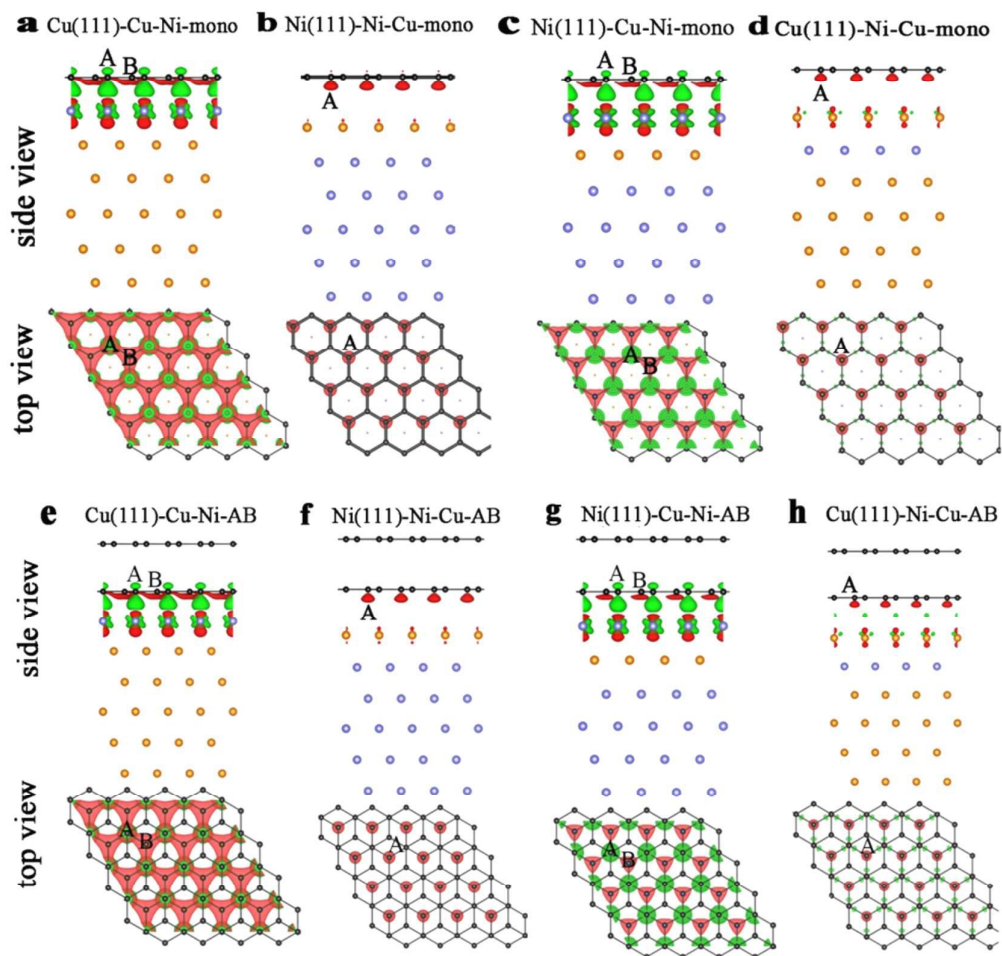


**Fig. 4** Charge density difference plots of mono- and bilayer graphene on Ni/Cu(111) SAs and NSAs. The charge density difference refers to the variance between the total charge density of graphene-Ni/Cu(111) systems and the sum of the charge density of the separated graphene and Ni/Cu(111) SA or NSA. The geometric structures of separated graphene and Ni/Cu(111) were kept the same as those in graphene-Ni/Cu(111) systems. The red and green color regions mark the depletion and accumulation of electronic charges, respectively. The top views show the charge density difference at interface of the graphene-Ni/Cu(111) systems.

To better illustrate the charge transfer at interface, the charge density differences of mono- and bilayer graphene on these Ni/Cu(111) SAs and NSAs are plotted in Fig. 4. As illustrated in Fig. 4a, c, e, and g, there is a strong charge transfer at the interface

between the graphene bottom layer and Ni-surface layer, resulting in strong chemical bonds between graphene layer and Ni-surface layer. For the monolayer graphene adsorption on the Cu(111)-Cu-Ni SA, the side view in Fig. 4a shows that the surface Ni atoms directly donate electrons to the C atoms sitting on top of the Ni atoms (labeled as A), and C atoms sitting on hollow sites (labeled as B) also back donate electrons from their  $\sigma$ -bands. The top view in Fig. 4a shows that, on the monolayer graphene, the charge density significantly increases near C atoms at the position A, while its decreases near C atoms at the position B. The Bader charge analysis further confirms that C atoms at the position A have  $-0.22$  e/atom, while C atoms at the position B only have  $+0.06$  e/atom, respectively. For the Cu(111)-Cu-Ni SA, the charge depletions of surface Ni atoms is  $+0.14$  e/atom, while subsurface Cu atoms only deplete  $+0.02$  e/atom.

In comparison, the graphene/Ni(111)-Cu-Ni NSA system has a subtle difference with the graphene/Cu(111)-Cu-Ni SA system as shown in the top view of Fig. 4c and a. The side view in Fig. 4c shows that surface Ni atoms and C atoms at the position B donate their electrons to C atoms which at the position A together. The Bader charge analysis further confirms that C atoms at the position A have  $-0.21$  e/atom, while C atoms at the position B have  $+0.12$  e/atom. The surface Ni atoms only deplete  $+0.06$  e/atom. The subsurface Cu atoms and third Ni atoms have  $+0.05$ , and  $-0.02$  e/atom, respectively.

For the graphene adsorption on the Cu-surface systems, there is only a minor charge redistribution and electronic polarization at interface between the bottom layer and Cu-surface layer, which can be observed less charge accumulation on the C atom at the position A as shown in Fig. 4b and d. On both Ni-surface and Cu-surface systems, the charge transfer of the bottom layer of bilayer graphene is similar to the

monolayer graphene. The top layer of bilayer graphene has neither charge accumulation nor depletion, as shown in Fig. 4e, g, f, and h.

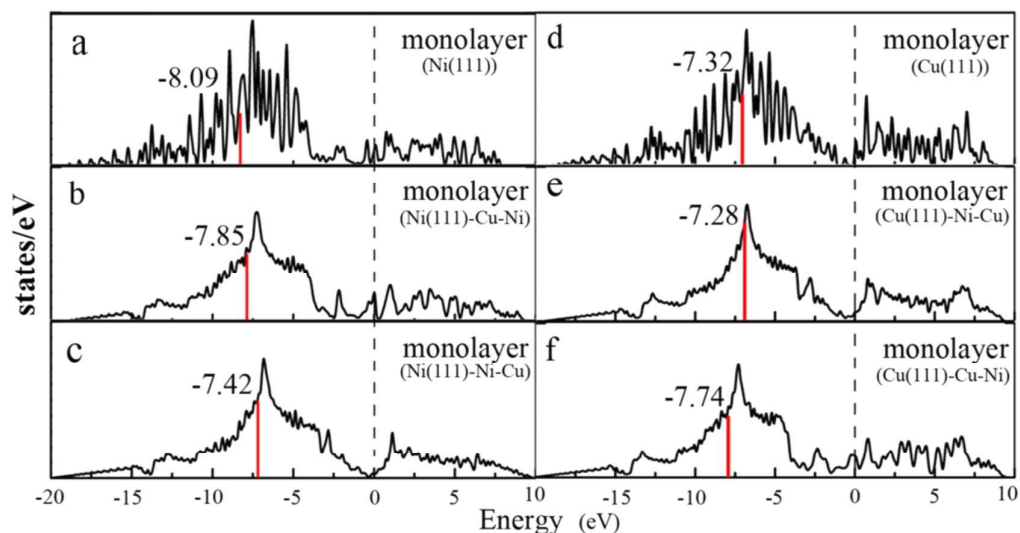


**Fig. 5** The DOS onto the P-band of the monolayer graphene on Ni(111), Cu(111) and Ni/Cu(111) SAs and NSAs. The red lines indicate the corresponding P-band center (eV). The dash lines indicate the Fermi level, which is taken as zero.

#### Partial density of states of graphene on the Ni/Cu(111) SAs and NSAs

It is well known that P-band of graphene is related to the interaction between graphene layer and metal surfaces. In order to have a better insight into the interaction of graphene with Ni/Cu(111) SAs and NSAs, herein, the p-band centers of monolayer graphene in these graphene/metal systems are plotted. A good relationship between the p-band centers of monolayer graphene and the interaction strength of graphene-metal is found by comparing the adsorption energies in Table 3 and the p-band centers in Fig. 5. The p-band centers of monolayer graphene are -7.42 eV on Ni(111)-Ni-Cu and -7.85 eV on Ni(111)-Cu-Ni, while it is -8.09 eV on Ni(111) as shown in Fig. 5c, b, and a. As a consequence, the interaction energies of graphene on these metal substrates are also in the order of Ni(111)-Ni-Cu < Ni(111)-Cu-Ni < Ni(111) as shown in Table 3. Obviously, there is a larger upshift of p-band center in

monolayer graphene on Ni/Cu(111) SAs and NSAs than that on the Ni(111), indicating a higher chemical activity and relatively weaker interaction of monolayer graphene on Ni/Cu(111) SAs and NSAs than that on the Ni(111). For the Cu-based SAs and NSAs, the p-band center of monolayer graphene on Cu(111)-Cu-Ni is  $-7.74$  eV, exhibit a downshift compared to that on Cu(111) ( $-7.32$  eV) as shown in Fig. 5f and d, indicating a lower chemical activity and stronger interaction of graphene on Cu(111)-Cu-Ni SA than that on Cu(111). However, the change of p-band center is not obvious for graphene on Cu(111)-Ni-Cu ( $-7.28$  eV) compared to that on the Cu(111) ( $-7.32$  eV) as shown in Fig. 5e and d. The adsorption energies of graphene on these metal substrates are in the order of Ni(111)-Ni-Cu > Cu(111)-Ni-Cu  $\approx$  Cu(111) as shown in Table 3.

## Discussion

Epitaxial growth of graphene on transition metal surfaces is a complex heterogeneous catalytic process. Transition metal surfaces usually serve as a support for chemical vapor deposition growth of graphene. It is generally accepted that C precursors would decompose and deposit carbon atoms or dimers on the metal surfaces. And then C atoms or dimers would nucleate to form small C clusters of various sizes. Subsequently, these C atoms or dimers on metal catalysts continuously incorporate into C clusters, and eventually grow into graphene layer on metal surfaces. Many experimental and theoretical studies have showed that in general graphene displays two distinct types of interaction with transition metal surfaces. Graphene may chemisorb on metal surface through a hybridization between the  $\pi$ -orbital of graphene and d-orbital of metal with graphene-metal distance of  $\sim 2.1$  Å. This happens on Ni, Co, Ru, and Pd.<sup>50</sup> In contrast, the distance between graphene and the metal surface is  $\sim 3.0$  Å. When graphene physisorbs on the Cu, Pt, Ag, and Au

surfaces through Pauli-exclusion and van der Waals (vdW) attraction between the  $\pi$ -orbital of graphene and s-orbital of metal.<sup>51</sup>

The intention of our recent works is to find a general guideline for layer controlled growth of graphene on metal surfaces by exploring the interfacial structure and interaction between graphene and metal surfaces. Our recent theoretical study shows that the interaction strength increases with the increase of graphene layers on the chemisorbed Ni(111) surface, while it decreases on the physisorbed Cu(111) surface.<sup>25</sup> Monolayer graphene on the Ni(111) is more reactive than that on the Cu(111). Furthermore, our results suggested that graphene growth on chemisorbed metal surface would lead to few-layer graphene; while the growth on physisorbed metal surfaces could be limited to mono- or bilayer graphene. In order to achieve layer controlled growth, it is important to be able to tune the interaction between graphene and metal surfaces during different growth stages. This could be done through doping metal surfaces with impurities or forming metal alloys.<sup>23, 52</sup>

In current work, to further explore the interaction of graphene layers with bimetallic alloys and their difference with the pure metal surfaces for controlled growth of graphene, we extended our study to investigate the interfacial structure and interaction of graphene layers with the bimetallic Ni/Cu(111) SA and NSAs. Our results from geometric structure, adsorption energy, charge transfer, and DOS demonstrate that the interaction strength between graphene layer and bimetallic surface could be tuned selectively by reasonable designing surface alloys. The initially weak interfacial interaction of graphene/Cu(111) could be enhanced substantially by Ni surface introducing. In contrast, the initially strong interfacial interaction of graphene/Ni(111) could be reduced successfully by Cu surface introducing. More interestingly, Liu et al. proposed a new pathway of layer control

growth of high-quality graphene that is the synergetic combination of the distinct carbon solubilities of Cu and Ni and well-known segregation phenomenon in Cu/Ni binary alloy.<sup>23</sup> Based on the finding from this study, we propose that the Ni layers located at subsurface could be used as the carbon source and layer number controlled, while the Cu layer located at surface could be employed as a favorable segregation medium, such as the Ni(111)-Ni-Cu SA. To achieve layer controlled growth of uniform graphene, this can be done through regulating the thickness of the surface Cu layers in the Ni(111)-Ni-Cu SA, so the segregation of carbon species on the Cu surface layers may be changed to provide desired growth condition.

### Conclusions

In this work, we systematically studied the properties of the Ni/Cu (111) SAs and NSAs and the interaction of the graphene layers with these Ni/Cu (111) SAs and NSAs by the DFT-D2 method. The results show that the Ni/Cu(111) SAs and NSAs have a larger surface relaxation than the Ni(111) and Cu(111). The interlayer distance increases when a Ni layer of the Ni(111) is substituted with a Cu layer, while it decreases when a Cu layer of the Cu(111) is substituted with a Ni layer. Furthermore, the Ni/Cu(111) SA/NSAs with the Cu-surface layer is energetically more favorable than that with the Ni-surface layer. Charge density difference and Bader charge analysis show that the interfacial layers of the Ni/Cu (111) SAs and NSAs exhibit different charge transfer distinctly. Charge always transfers from the Cu-layer to Ni-layer, leading to Ni-layer with more charge accumulation than Cu-layer. The results of DOS suggest that the Ni-surface layer of the Ni/Cu(111) SA/NSAs have a higher chemical activity than the Cu-surface layer.

When graphene layers adsorb on these Ni/Cu(111) SAs and NSAs, the interaction behavior directly depends on the adjoining surface-metal layer. Thereby,

the interaction strength of graphene-metal can be tuned by the surface alloying distinctly, while it has only minor change by subsurface alloying. The initially weak interfacial interaction of graphene/Cu(111) could be enhanced substantially by Ni surface introducing. The interface distance was decreased from  $\sim 3.0$  Å to  $\sim 2.1$  Å, and there is a strong charge transfer from the Ni-surface layer to graphene bottom layer. In contrast, the initially strong interfacial interaction of graphene/Ni(111) could be reduced successfully by Cu surface introducing. Accordingly, the interface distance was increased from  $\sim 2.1$  Å to  $\sim 3.0$  Å, and there is only a minor electronic polarization at interface of graphene/Ni(111)-Ni-Cu. Furthermore, the analysis of DOS shows that the graphene bottom layer on Ni-surface layer has higher chemical activity than that on Cu-surface layer. The deeper insights into the interfacial structure and interaction between graphene layers and bimetallic SAs and NSAs from this study are expected to provide guides for designing alloy catalyst and achieving controlled growth of graphene.

### Acknowledgments

We acknowledge financial supports by National Natural Science Foundations of China (21373112, 21203094, 11574062) and China Postdoctoral Science Foundation (2016M591834).

### References

- 1 R. G. Van Wesep, H. Chen, W. Zhu and Z. Zhang, *J. Chem. Phys.*, 2011, 134, 171105.
- 2 K. S. Kim, Y. Zhao, H. Jang, S. Y. Lee, J. M. Kim, K. S. Kim, J.-H. Ahn, P. Kim, J.-Y. Choi and B. H. Hong, *Nature*, 2009, 457, 706-710.
- 3 H. Chen, W. Zhu and Z. Zhang, *Phys. Rev. Lett.*, 2010, 104, 186101.
- 4 X. Li, W. Cai, J. An, S. Kim, J. Nah, D. Yang, R. Piner, A. Velamakanni, I. Jung, E. Tutuc, S. K. Banerjee, L. Colombo and R. S. Ruoff, *Science*, 2009, 324,

- 1312-1314.
- 5 A. Reina, X. Jia, J. Ho, D. Nezich, H. Son, V. Bulovic, M. S. Dresselhaus and J. Kong, *Nano Lett.*, 2009, 9, 30-35.
  - 6 J. Lahiri, T. Miller, L. Adamska, I. I. Oleynik and M. Batzill, *Nano Lett.*, 2011, 11, 518-522.
  - 7 S. Helveg, C. Lopez-Cartes, J. Sehested, P. L. Hansen, B. S. Clausen, J. R. Rostrup-Nielsen, F. Abild-Pedersen and J. K. Nørskov, *Nature*, 2004, 427, 426-429.
  - 8 G. H. Han, F. Guenes, J. J. Bae, E. S. Kim, S. J. Chae, H.-J. Shin, J.-Y. Choi, D. Pribat and Y. H. Lee, *Nano Lett.*, 2011, 11, 4144-4148.
  - 9 H. Ji, Y. Hao, Y. Ren, M. Charlton, W. H. Lee, Q. Wu, H. Li, Y. Zhu, Y. Wu, R. Piner and R. S. Ruoff, *ACS Nano*, 2011, 5, 7656-7661.
  - 10 H. I. Rasool, E. B. Song, M. Mecklenburg, B. C. Regan, K. L. Wang, B. H. Weiller and J. K. Gimzewski, *J. Am. Chem. Soc.*, 2011, 133, 12536-12543.
  - 11 S. Yoshii, K. Nozawa, K. Toyoda, N. Matsukawa, A. Odagawa and A. Tsujimura, *Nano Lett.*, 2011, 11, 2628-2633.
  - 12 S. Guenther, S. Daenhardt, B. Wang, M. L. Bocquet, S. Schmitt and J. Winterlin, *Nano Lett.*, 2011, 11, 1895-1900.
  - 13 J. Coraux, A. T. N'Diaye, C. Busse and T. Michely, *Nano Lett.*, 2008, 8, 565-570.
  - 14 J. Coraux, A. T. N'Diaye, M. Engler, C. Busse, D. Wall, N. Buckanie, F.-J. M. z. Heringdorf, R. van Gastel, B. Poelsema and T. Michely, *New J. Phys.*, 2009, 11, 039801.
  - 15 S. Chen, W. Cai, R. D. Piner, J. W. Suk, Y. Wu, Y. Ren, J. Kang and R. S. Ruoff, *Nano Lett.*, 2011, 11, 3519-3525.
  - 16 K. Yan, H. Peng, Y. Zhou, H. Li and Z. Liu, *Nano Lett.*, 2011, 11, 1106-1110.
  - 17 S. Entani, Y. Matsumoto, M. Ohtomo, P. V. Avramov, H. Naramoto and S. Sakai, *J. Appl. Phys.*, 2012, 111, 064324.
  - 18 P. Avouris and C. Dimitrakopoulos, *Mater. Today*, 2012, 15, 86-97.
  - 19 Y. Yao, Z. Li, Z. Lin, K.-S. Moon, J. Agar and C. Wong, *J. Phys. Chem. C*, 2011, 115, 5232-5238.
  - 20 H. Zhang, Y. Zhang, B. Wang, Z. Chen, Y. Sui, Y. Zhang, C. Tang, B. Zhu, X. Xie, G. Yu, Z. Jin and X. Liu, *J. Electron. Mater.*, 2015, 44, 79-86.
  - 21 N. R. Wilson, A. J. Marsden, M. Saghir, C. J. Bromley, R. Schaub, G. Costantini, T. W. White, C. Partridge, A. Barinov, P. Dudin, A. M. Sanchez, J. J. Mudd, M. Walker and G. R. Bell, *Nano Res.*, 2013, 6, 99-112.
  - 22 T. Chanier and L. Henrard, *Eur. Phys. J. B*, 2015, 88, 31.
  - 23 X. Liu, L. Fu, N. Liu, T. Gao, Y. Zhang, L. Liao and Z. Liu, *J. Phys. Chem. C*, 2011, 115, 11976-11982.
  - 24 D. Cheng and K. Jiang, *Surf. Sci.*, 2013, 609, 85-90.
  - 25 Q. Wang, L. Wei, M. Sullivan, S.-W. Yang and Y. Chen, *Rsc Adv.*, 2013, 3, 3046-3053.
  - 26 A. B. Preobrajenski, M. L. Ng, A. S. Vinogradov and N. Martensson, *Phys. Rev. B*, 2008, 78, 073401.

- 27 J. Sanchez-Barriga, A. Varykhalov, M. R. Scholz, O. Rader, D. Marchenko, A. Rybkin, A. M. Shikin and E. Vescovo, *Diam. Relat. Mater.*, 2010, 19, 734-741.
- 28 D. Eom, D. Prezzi, K. T. Rim, H. Zhou, M. Lefenfeld, S. Xiao, C. Nuckolls, M. S. Hybertsen, T. F. Heinz and G. W. Flynn, *Nano Lett.*, 2009, 9, 2844-2848.
- 29 B. Dai, L. Fu, Z. Zou, M. Wang, H. Xu, S. Wang and Z. Liu, *Nat. Commun.*, 2011, 2, 522.
- 30 R. Addou, A. Dahal and M. Batzill, *Surf. Sci.*, 2012, 606, 1108-1112.
- 31 R. S. Weatherup, B. C. Bayer, R. Blume, C. Ducati, C. Baetz, R. Schloegl and S. Hofmann, *Nano Lett.*, 2011, 11, 4154-4160.
- 32 Y. S. Dedkov, A. M. Shikin, V. K. Adamchuk, S. L. Molodtsov, C. Laubschat, A. Bauer and G. Kaindl, *Phys. Rev. B*, 2001, 64, 035405.
- 33 M. H. Kang, S. C. Jung and J. W. Park, *Phys. Rev. B*, 2010, 82, 085409.
- 34 Y. S. Dedkov and M. Fonin, *New J. Phys.*, 2010, 12, 125004.
- 35 S. Grimme, *J. Comput. Chem.*, 2006, 27, 1787-1799.
- 36 T. Bucko, J. Hafner, S. Lebegue and J. G. Angyan, *J. Phys. Chem. A*, 2010, 114, 11814-11824.
- 37 P. E. Blochl, *Phys. Rev. B*, 1994, 50, 17953-17979.
- 38 G. Kresse and D. Joubert, *Phys. Rev. B*, 1999, 59, 1758-1775.
- 39 G. Kresse and J. Furthmuller, *Phys. Rev. B*, 1996, 54, 11169-11186.
- 40 J. P. Perdew, K. Burke and Y. Wang, *Phys. Rev. B*, 1996, 54, 16533-16539.
- 41 M. Fuentes-Cabrera, M. I. Baskes, A. V. Melechko and M. L. Simpson, *Phys. Rev. B*, 2008, 77, 035405.
- 42 J. P. Perdew, K. Burke and M. Ernzerhof, *Phys. Rev. Lett.*, 1996, 77, 3865-3868.
- 43 M. Vanin, J. J. Mortensen, A. K. Kelkkanen, J. M. Garcia-Lastra, K. S. Thygesen and K. W. Jacobsen, *Phys. Rev. B*, 2010, 81, 081408.
- 44 I. Hamada and M. Otani, *Phys. Rev. B*, 2010, 82, 153412.
- 45 A. H. Macdonald, *Phys. Rev. B*, 1978, 18, 5897-5899.
- 46 E. Sanville, S. D. Kenny, R. Smith and G. Henkelman, *J. Comput. Chem.*, 2007, 28, 899-908.
- 47 G. Henkelman, A. Arnaldsson and H. Jonsson, *Comp. Mater. Sci.*, 2006, 36, 354-360.
- 48 G. Held, *Appl. Phys. A*, 2003, 76, 689-700.
- 49 J.-H. Lin and V. V. Guliyants, *Appl. Catal. a-Gen.*, 2012, 445, 187-194.
- 50 P. A. Khomyakov, G. Giovannetti, P. C. Rusu, G. Brocks, J. van den Brink and P. J. Kelly, *Phys. Rev. B*, 2009, 79, 195425.
- 51 G. Giovannetti, P. A. Khomyakov, G. Brocks, V. M. Karpan, J. van den Brink and P. J. Kelly, *Phys. Rev. Lett.*, 2008, 101, 026803.
- 52 S. M. Kozlov, F. Vines and A. Goerling, *J. Phys. Chem. C*, 2012, 116, 7360-7366.